J Geod (2014) 88:839–855
DOI 10.1007/s00190-014-0725-9

ORIGINAL ARTICLE

Secular changes in Earth's shape and surface mass loading derived from combinations of reprocessed global GPS networks

David Booker · Peter J. Clarke · David A. Lavallée

Received: 1 July 2013 / Accepted: 15 April 2014 / Published online: 6 May 2014

Abstract The changing distribution of surface mass (oceans, atmospheric pressure, continental water storage, groundwater, lakes, snow and ice) causes detectable changes in the shape of the solid Earth, on time scales ranging from hours to millennia. Transient changes in the Earth's shape can, regardless of cause, be readily separated from steady secular variation in surface mass loading, but other secular changes due to plate tectonics and glacial isostatic adjustment (GIA) cannot. We estimate secular station velocities from almost 11 years of high quality combined GPS position solutions (GPS weeks 1,000–1,570) submitted as part of the first international global navigation satellite system service reprocessing campaign. Individual station velocities are estimated as a linear fit, paying careful attention to outliers and offsets. We remove a suite of a priori GIA models, each with an associated set of plate tectonic Euler vectors estimated by us; the latter are shown to be insensitive to the a priori GIA model. From the coordinate time series residuals after removing the GIA models and corresponding plate tectonic velocities, we use mass-conserving continental basis functions to estimate surface mass loading including the secular term. The different GIA models lead to significant differences in the estimates of loading in selected regions. Although our loading estimates are broadly comparable with independent estimates from other satellite missions, their range highlights the need for better, more robust GIA models that incorporate 3D Earth structure and accurately represent 3D surface displacements.

Keywords Geodesy · International GNSS service (IGS) reprocessing campaign · Surface mass loading · Secular change

1 Introduction

The changing distribution of surface masses causes detectable changes to the shape of the Earth, on timescales from hours to millennia. These changes manifest in the station positions recorded using global navigation satellite systems (GNSS), including the global positioning system (GPS). If this deformation can be detected, isolated, and quantified, then inferences can be made regarding large-scale surface mass redistribution and the Earth's elastic response. These inferences will affect how any terrestrial reference frame (TRF) is realised, in turn influencing uses of the TRF such as satellite altimetry missions, GIA modelling, and global tide gauge monitoring for sea level change detection. Previous studies into these effects include surface mass loading (Clarke et al. 2007; van Dam et al. 2007, 2001), plate tectonics (Larson et al. 1997; Kogan and Steblov 2008) and GIA (e.g. Milne et al. 2004). However, there are some doubts in the quality of the TRF used in these early studies. This paper presents results of the combination of the first IGS reprocessing campaign and analysis of surface mass loading using this catalogue of data which has been shown to be vastly superior to the operational IGS processing and other earlier analyses (Collilieux et al. 2011). By virtue of the fact that we form a combined solution

Electronic supplementary material The online version of this article (doi:10.1007/s00190-014-0725-9) contains supplementary material, which is available to authorized users.

D. Booker · P. J. Clarke (✉)
School of Civil Engineering and Geosciences, Newcastle University, Cassie Building, Newcastle-upon-TyneNE1 7RU, UK
e-mail: peter.clarke@newcastle.ac.uk

D. A. Lavallée
Shell International Exploration and Production Inc., Shell Technology Center, Houston, 3333 Highway 6 South, Houston, TX 77082, USA

which inherently mitigates errors that may be present in any individual GPS analysis package, our dataset has advantages over other more recent global solutions (Tregoning and Watson 2009; Tesmer et al. 2011) even though these too are considerable improvements on historical work. The data used in this series spans GPS week 1,000–1,570 which corresponds to nearly 11 years (March 1999–February 2010) of weekly observations of station coordinates. By removing plate tectonic and GIA motions, and inverting the residual velocities using a set of gravitational consistent mass-conserving basis functions it is possible to estimate present-day surface mass change.

2 Geophysical causes of deformation

The deformation of the solid Earth occurs over a range of time scales, from the very high frequency (sub-daily) to the extremely long, spanning centuries. Signals appear seasonally and inter-seasonally (van Dam and Francis 1998; van Dam et al. 2001; Cretaux et al. 2002; Bennett 2008; Bos et al. 2008) and over transient (Arriagada et al. 2011; Chen et al. 2011; Reddy et al. 2011) and secular (Larson et al. 1997; Mitrovica et al. 1994; Wahr et al. 2001; Khan et al. 2008) time scales. The focus of this study is on the secular trends, in particular the estimation of present-day surface mass loading (SML). The secular motion of any point on the Earth will be a combination of GIA, plate tectonics, present-day surface mass loading, and other secular effects which we here assume to be negligible (Eq. 1).

$$\dot{X} = \dot{X}_{\mathrm{GIA}} + \dot{X}_{\mathrm{Tectonics}} + \sum X_{\mathrm{SML}} + \dot{X}_{\mathrm{Other}} \tag{1}$$

By removing a model which is a combination of an a priori GIA model (Sect. 2.1) and an associated estimate of plate tectonic movement (Sect. 2.2), the residual velocity should be due solely to present-day secular SML, plus of course any observation and model errors and other effects assumed to be negligible. It has been shown that geodetic displacement data can be inverted to infer surface mass loading (e.g. Blewitt and Clarke 2003; Wu et al. 2003). The total load on the surface of the Earth, T, can be expressed in equivalent terms of a column of sea water, density ρ_s as a function of location Ω (latitude ϕ, longitude λ):

$$T(\Omega) = \sum_{n=1}^{\infty} \sum_{m=1}^{n} \sum_{\Phi}^{\{C,S\}} T_{nm}^{\Phi} Y_{nm}^{\Phi}(\Omega) \tag{2}$$

where Y_{nm}^{Φ} are spherical harmonic functions of degree n, order m, phase Φ.

Equation (2) describes the total load upon the surface of the Earth. The vertical (H) and lateral (E and N) elastic displacements induced by $T(\Omega)$ can be calculated using the load Love numbers (Love 1909).

$$\begin{aligned}
H(\Omega) &= \frac{3\rho_s}{\rho_E} \sum_{n=1}^{\infty} \sum_{m=1}^{n} \sum_{\Phi}^{\{C,S\}} \frac{h_n'}{2n+1} T_{nm}^{\Phi} Y_{nm}^{\Phi}(\Omega) \\
E(\Omega) &= \frac{3\rho_s}{\rho_E} \sum_{n=1}^{\infty} \sum_{m=1}^{n} \sum_{\Phi}^{\{C,S\}} \frac{l_n'}{2n+1} T_{nm}^{\Phi} \frac{\partial_\lambda Y_{nm}^{\Phi}(\Omega)}{\cos\phi} \\
N(\Omega) &= \frac{3\rho_s}{\rho_E} \sum_{n=1}^{\infty} \sum_{m=1}^{n} \sum_{\Phi}^{\{C,S\}} \frac{l_n'}{2n+1} T_{nm}^{\Phi} \partial_\phi Y_{nm}^{\Phi}(\Omega)
\end{aligned} \tag{3}$$

The standard spherical harmonics $Y_{nm}^{\Phi}(\Omega)$ have been used to estimate very low-degree surface mass loading from GPS displacements (e.g. Blewitt et al. 2001); however, they become insufficient at higher degrees without additional constraints as they do not distinguish between continental and oceanic mass storage. The standard spherical harmonic coefficients allow equally large loads to distribute over the oceans and continents. However, because the ocean is free to redistribute over time scales of a few days and longer, the magnitude of the secular (i.e. non-tidal) ocean load change is very small compared to the localised loads that may be induced upon the continents. Furthermore, there is relatively little GPS data to constrain the oceanic domain, and so the inverse problem rapidly becomes unstable at higher degrees (Clarke et al. 2007; Wu et al. 2002). By assuming that mass is conserved globally and that the oceans follow the gravitationally consistent sea level equation (SLE) (Farrell and Clark 1976) it is possible to estimate the load without additional data. In this paper, the standard spherical harmonic coefficients are replaced with the gravitationally consistent, mass-conserving basis functions of Clarke et al. (2007).

2.1 Glacial isostatic adjustment

GIA is the response of the Earth to changes in global ice coverage, which reached its maximum during the last ice age covering large areas of North America, Eurasia and Antarctica. When ice rests on the Earth's surface, the load on the crust deforms the lithosphere downwards into the asthenospheric upper mantle. This causes viscous flow laterally away from the centre of the load. Retreat or thinning of the ice allows the mantle material to redistribute towards its pre-load isostatic equilibrium. It is this movement of mantle material which transmits through the crust causing a 3D displacement of the surface which is the signature of present-day GIA. This effect is a significant one, especially in the vertical direction. In this paper we will consider two example GIA models, the 'Prime' and 'Alt' models of (Schotman et al. 2008), to compare their effect on estimates of plate tectonic motion and present-day surface mass transfer. The models are provided as 3D displacements on a $1^\circ \times 1^\circ$ grid.

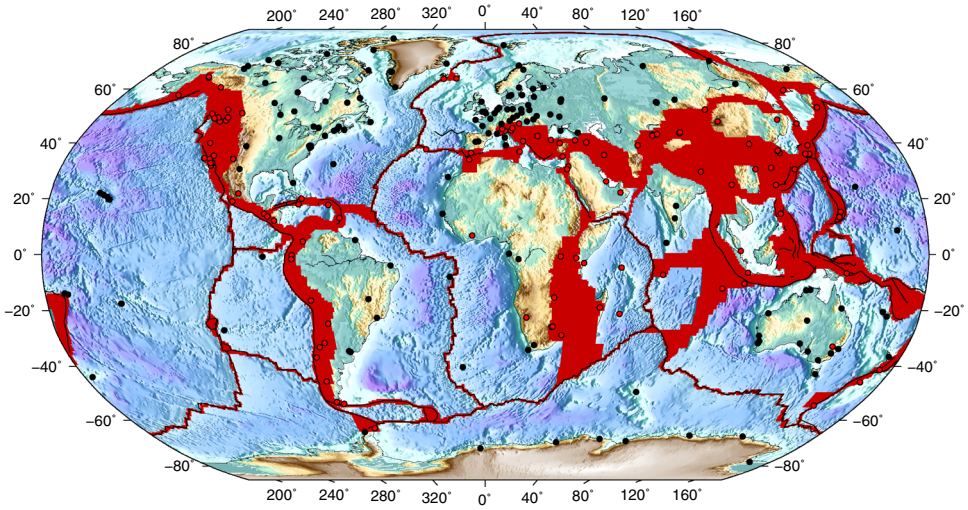

Fig. 1 Station network distribution. *Solid circles* are included stations, *open circles* represent rejected stations due to proximity to plate boundary deformation zones [*red* hatching, Kreemer et al. (2000)]

A GIA model is formed from two input models: the Earth model and the ice history. The Schotman models use a modified ICE3G history (Tushingham and Peltier 1991), with the last glacial maximum (LGM) at 21.5 kyr BP and ice-free conditions from 4 kyr BP. As this study is concerned with present-day mass loss, the (unmodelled) GIA response to any ice mass movement which occurred after the end of the modelled period will tend to bias our estimates. The second input into a GIA model is the Earth model; this describes the viscous and elastic parameters of the Earth at intervals varying with depth. The Schotman Earth model is a basic stepwise model modified from PREM, containing five distinct bands. The alternative Schotman model has a thinner lithosphere of 98 km and a uniform mantle viscosity. Schotman et al. (2008) note that there is no empirical evidence for this variation to the Earth model but it is provided as a comparison. These Earth models are only 1D, with viscosity varying only with depth. It has been shown that the Earth's viscosity also varies laterally and these variations should be modelled to accurately describe GIA velocities (King et al. 2010). There have been preliminary studies (Paulson et al. 2005; Kendall et al. 2006; Davis et al. 2008) into 3D Earth models which introduce lateral variations in viscosity, but to date there has been no commonly adopted 3D Earth model. This known model deficiency, and potential errors in the ice history, will cause errors in the estimates of present-day GIA surface velocities. However, by considering more than one GIA model it remains possible to gauge the approximate bounds of any such errors.

2.2 Plate tectonics

The second secular velocity introduced into each coordinate time series is due to the movements of the tectonic plates. The tectonic plates are free to rotate as rigid bodies over the surface of the Earth, leading to motion $\mathbf{v}$ in the horizontal plane at each location $\mathbf{r}$ (all vectors are Cartesian geocentric quantities):

$$\begin{aligned}\mathbf{v} &= \Omega \times \mathbf{r} \\ &= \omega \mathbf{e} \times \mathbf{r}\end{aligned} \tag{4}$$

where Ω is the Euler rotation vector for the plate containing location $\mathbf{r}$, with magnitude ω about an axis specified by unit vector $\mathbf{e}$ which points towards the plate's Euler pole. In total our dataset includes 289 stations which meet the observation time span criteria of Blewitt and Lavallee (2002). Figure 1 shows the distribution of potential candidate sites to be used in the inversion of Eq. (4).

Additional vertical and lateral deformation, both transient and secular, occurs close to a tectonic plate boundary and these locations therefore cannot be modelled using the plate's Euler vector. There is also the potential for position offsets introduced by seismic activity at the plate boundary, which will affect the estimate of secular velocity if uncorrected. It is for these reasons that only stations which are located on the rigid plate interior will be used for the Euler vector estimation. After filtering for station location there are 172 stations which are deemed to be located on the rigid plate interiors. These stations are represented by orange circles in Fig. 1. Each must be assigned to an individual tectonic plate (see discussion later).

3 IGS reprocessing campaign

Since the inception of the IGS and GPS constellation, various working groups have been striving to produce and publish a variety of products all derived from the GPS tracking network data (Dow et al. 2009). One of these products is a weekly station coordinate global network solution produced by participating analysis centres (ACs) in the SINEX

Table 1 IGS Analysis centres and their software

AC	Full name	ID	Software
CODE	Centre for Orbit Determination Europe	CO1	Bernese
EMR	Natural Resources Canada	EM1	GIPSY
ESA	European Space Agency	ES1	NAPEOS
GFZ	GeoForschungZentrum	GF1	EPOS
GFZ	GeoFroschungZentrum	GT1	EPOS
JPL	Jet Propulsion Laboratory	JP1	GIPSY
MIT	Massachusetts Institute of Technology	MI1	GAMIT
NGS	National Geodetic Survey	NG1	Pages
PDR	Potsdam/TU Dresden	PD1	GAMIT
SIO	Scripps Institute of Technology	SI1	GAMIT

GIPSY, NAPEOS and Pages use an undifferenced approach; Bernese, GAMIT and EPOS use a double differenced approach

Table 2 Significant differences of IGS reprocessing models compared with operational IGS processing before GPS week 1,452

Model
Absolute satellite and receiver antenna calibrations (Schmid et al. 2005)
IGS05 reference frame (Ferland and Piraszewski 2009)
Updated IERS conventions 2003 (McCarthy and Petit 2004)
Updated Ocean tide loading model FES2004 (Ray et al. 2004)
No non-tidal loading displacements
Updated tropospheric propagation delay models (Boehm et al. 2006)
No higher order ionospheric effects applied
Updated IGS catalogue to include historic and defunct IGS stations
P1-C1 satellite code bias corrections (Schaer 2006)

For further details see http://acc.igs.org/reprocess.html

format. As part of the processing, a priori reference models accounting for known effects such as ocean tides and atmospheric propagation are incorporated; these models are continually improving and being updated. A disadvantage of these model improvements is the introduction of systematic offsets in the operational weekly solutions, making studies into secular trends extremely difficult. The changes which have had the largest noticeable effects are the combined adoption of the IGS05 coordinate reference frame (Ferland and Piraszewski 2009) and the switch from relative to absolute antenna phase centre variations (Schmid et al. 2005). The first IGS reprocessing campaign (http://acc.igs.org/reprocess.html) was a concerted effort by IGS institutions to reprocess all available GPS data using the latest analysis techniques. The aim of the reprocessing campaign is to produce a homogeneous set of time series using the most up-to-date analysis models. Table 1 lists all the ACs taking part in the reprocessing campaign which have been used in this study. Each AC is free to choose the processing software, GNSS system(s), analysis strategy (within limits) and number of stations included. In addition to the ACs, several institutions (Natural Resources Canada (NRCan), Newcastle University, MIT and the Institut Géographique National) were responsible for producing combined solutions, with the NRCan solution adopted as the official IGS product included in the ITRF2008 (Altamimi et al. 2011).

The models used in the reprocessing campaign are those used in the current operational IGS processing since GPS week 1,452, and are listed in Table 2. There are two solutions from GFZ; one of these is the regular GPS AC submission, the second (GT1) is a tide gauge (TIGA) solution.

3.1 Network combination

There are several institutions tasked with the combination of individual AC SINEX files. The official operational network combination for the IGS is now based at the IGN (Collilieux et al. 2011) using the CATREF software. The results in this paper are produced at Newcastle University using the bespoke software TANYA (Davies and Blewitt 2000). TANYA uses a robust least squares (LS) combination, aligning each weekly solution via a 7-parameter Helmert transformation to the chosen reference frame rather than constraining it at individual sites, as the latter is known to introduce errors into the network (Blewitt et al. 1992). The single combined solution has been shown to be superior to any individual AC submission (Davies and Blewitt 2000). All AC submissions are given loose rotation constraints to aid inversion but these are removed in the final combination. The final combined weekly solutions are aligned to the IGS05 TRF (Altamimi et al. 2007). Whereas Collilieux et al. (2011) present the results from four reprocessed GPS ACs plus other geodetic techniques, this paper presents the results of ten reprocessed AC solutions (Table 1).

3.2 GPS station tracking network

The distribution of sites used in this study is shown in Fig. 1; however, not all stations appear in every weekly solution: stations drop out and reappear from week to week due to a variety of reasons such as temporary failures of equipment or communications. Figure 2 plots the number of stations included in each weekly solution. For the operational solution, especially at earlier epochs, stations may have been excluded because their data span did not at the time meet criteria of permanency. As the number of stations included in the weekly solution increases, so does the precision of the network solution. In the first few weeks, the number of stations in the operational network is rather small in comparison with the reprocessed solution. Only towards the end of the processing period does the number of included stations in the operational processing converge

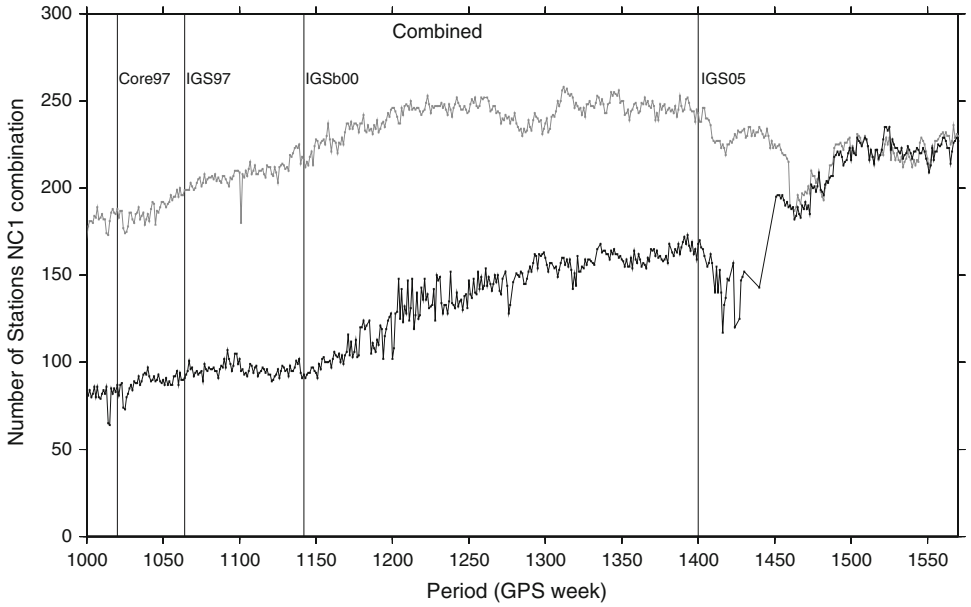

Fig. 2 Number of stations in each weekly network combination (*thick grey line* NC1 reprocessed solution; *thin black line* NCL operational solution). *Vertical black lines* represent adoption of new reference frames in the operational solution. Occasional outages of the NCL operational solution occurred during 2007 (weeks 1,400–1,452). After week 1,452, all underlying AC solutions are from the operational processing; minor differences occur between the results of operational and post-processed outlier detection

Table 3 Number of stations located on the rigid interior of each tectonic plate

Plate	Number of stations
Antarctica	9
Australia	24
Eurasia	62
India	4
Nazca	4
North America	41
Nubia	8
Pacific	12
South America	8
Total = 9	Total = 172

towards that of the reprocessing campaign, although it may not be identical because of data latency and outlier detection issues.

The IGS tracking network is a dynamic list of GNSS stations which has changed dramatically over the history of the IGS. Each AC is free to choose which stations to include in its weekly solutions. The IGS stipulates that each AC should include those that are present in a list of "Core" sites, but these are regularly supplemented with additional stations which may cover areas sparse of data or densify areas of interest. As discussed in Sect. 2.2, some of these sites are in close proximity to the tectonic plate boundary deformation zones. Once these potentially unusable sites have been filtered out, sites can be assigned to tectonic plates (Table 3).

In total there are 172 stations; however, the majority of these stations are located in Europe (62) or North America (41) creating an uneven distribution of sites between the northern and southern hemispheres. In our network there is enough data to be able to estimate Euler vectors for nine major plates. The Caribbean, Arabian, Amurian and Somalian plates do not contain sufficient plate interior sites to determine their Euler vectors, once sites have been rejected due to inconsistent velocities or extremely large coordinate residuals.

3.3 Quality of network combination

Several tests were carried out to ensure the quality of the combination. Initially any station which is present in >3 AC estimates is included and passed through a rigorous data snooping routine. Any station which has a normalised residual $>3\sigma$ based on the rescaled formal errors will be rejected from the combination; this test is iterated until no such outliers are present. This data snooping ensures that each weekly solution is stable within its own weekly frame. Comparing the reprocessed and operational weighted root mean square error (WRMS), each with respect to the chosen TRF, will highlight any improvement in the reprocessed solution, although for both solutions the WRMS will include the effect of any reference frame errors or nonlinear site motions that occur. Figure 3 shows the inhomogeneous nature of the operational processing in comparison to the reprocessing campaign. Every time a new reference frame or processing model is introduced it causes an systematic change in the long-term time series. It is these offsets in the data that make the study of secular deformation using the operational IGS solutions unreliable.

The parameters which are fundamental to any reference frame are the origin, orientation, and scale, and their time evolution. Each AC and combined solution is implicitly in

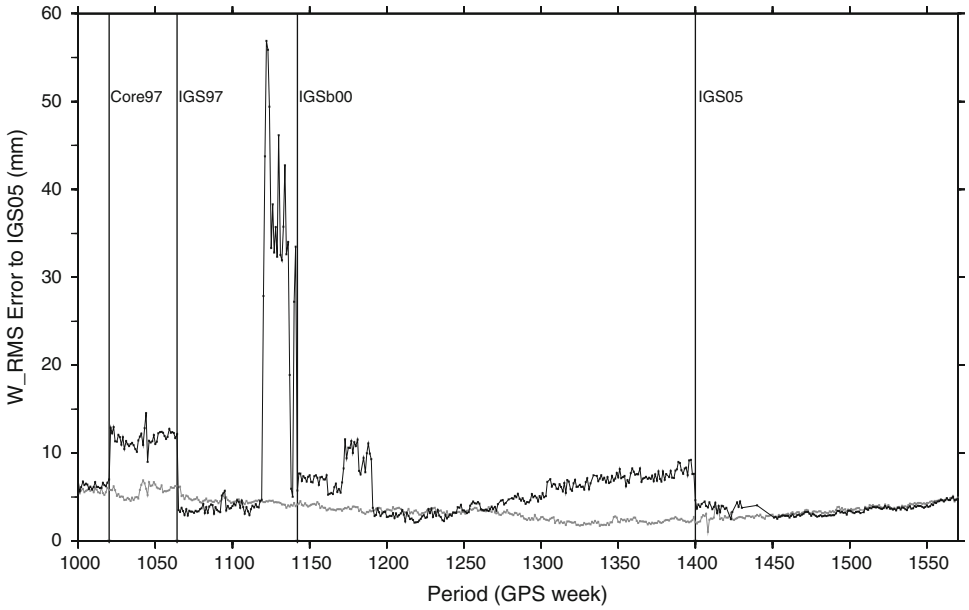

Fig. 3 Weighted RMS of weekly solutions: operational (*thin*, *black*) and reprocessed (*thick*, *grey*). *Black vertical lines* represents the adoption of a new reference frame in the operational processing

its own reference frame and as such they cannot be directly compared. To be able to compare solutions they first must be transformed to a common reference frame, in this case IGS05, via a 7-parameter Helmert transformation. The rotational parameters are not discussed as these result from conventional reference frame definition rather than physical measurement sensitivity, so they are not a measure of frame quality. Figure 4 shows that there is a high level of noise present in the operational combination which could potentially mask any signals; in comparison this noise is vastly (around 75 %) reduced in the reprocessed solution. This is due to several factors, including increased network density, improved processing models and the increased number of independent solutions. In addition to and as a result of the reduction in noise, a regular repeating signal becomes clear especially in the scale variation, which may be due to a number of effects including inter-hemispheric surface mass transfer (Collilieux et al. 2011).

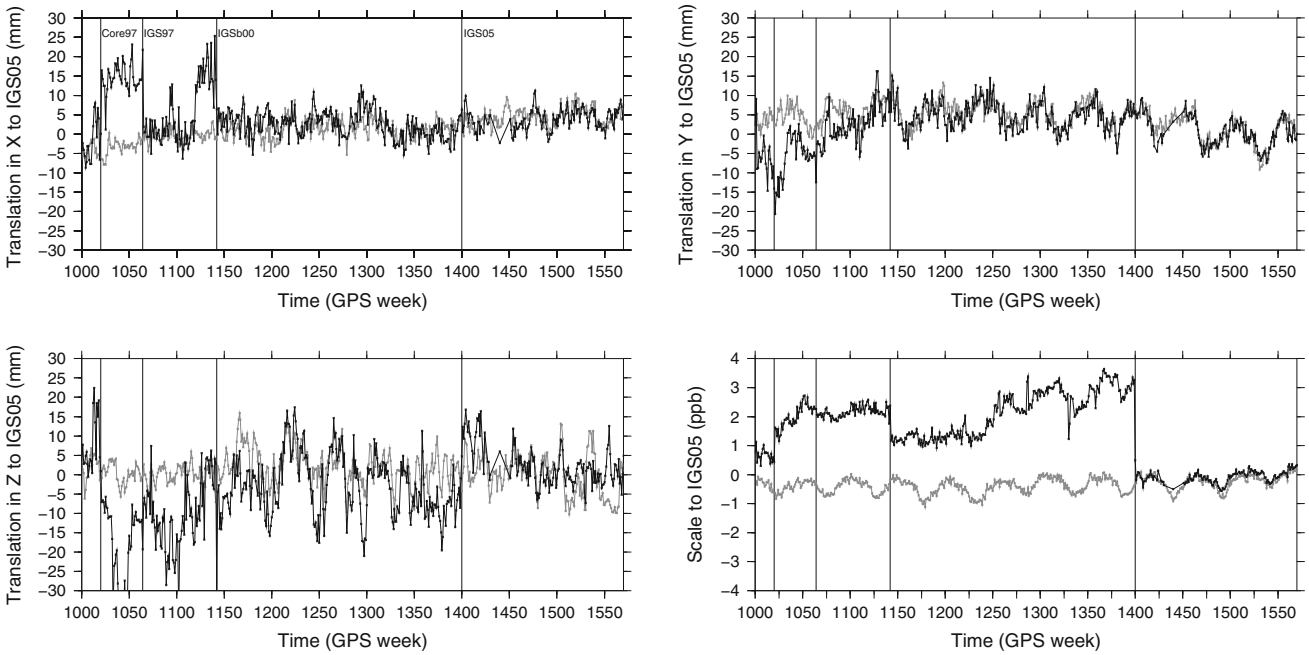

Fig. 4 Selected Helmert parameters relating operational (*thin*, *black*) and reprocessed (*thick*, *grey*) combination solutions to IGS05

4 Kinematic solution

For each station present in our "NC1" solution that meets the criteria of Blewitt and Lavallee (2002), i.e. a time span of >2.5 years and >104 weekly observations, a single three-dimensional velocity vector is calculated. This linear velocity encompasses secular trends due to GIA, plate tectonic movement, and present-day surface mass loading. Using an a priori GIA model and estimating and removing a corresponding plate tectonic model, a set of residual velocities can be calculated which should in principle relate only to secular present-day surface mass loading. In principle, it is conceivable that within the area of one of the smaller tectonic plates, a component of the surface mass loading deformation might resemble rigid-body motion and be absorbed into that plate's estimated Euler vector. This will not affect the residual vertical velocities and so the biasing effect on the estimated secular loading will be small. The variability in estimated Euler vectors using different GIA models, which give rise to similar regional deformation signals, will suggest approximate bounds on the possible magnitude of the effect.

Special care must be taken when dealing with outliers and offsets. Offsets may be caused by human (e.g. antenna or receiver) changes, or geophysical causes (e.g. earthquakes), and introduce a step into the station's motion. Offsets are identified via careful visual inspection; if the offset is due to equipment change then a simple offset can be estimated, whereas if it is due to a geophysical cause such as an earthquake then there may be a period of post-seismic deformation which must be removed as this does not represent the station's true long-term motion. The data snooping routine in the weekly combination concerned itself with station outliers with respect to the weekly solution. The second round of data snooping, in the kinematic solution, focuses on outliers in each individual station's long-term time series. This is achieved by inspecting the station's linear coordinate trend and the standard deviation of coordinates about this trend; if a weekly coordinate lies outside 3σ of the station's long-term progression then that station's weekly coordinates are rejected from the velocity estimation.

Through careful treatment of offsets and outliers, linear velocities of the selected 172 tracking stations have been calculated (Fig. 5). It is clear that sites move in the horizontal plane principally with the motions of the tectonic plates, and that the majority of vertical motion occurs near to areas that were previously glaciated. These velocities represent components of the raw secular motions of sites (Eq. 1).

4.1 Creating the model

We consider two example GIA models in this work, and also the "null GIA" model where no GIA velocity is subtracted. The process of producing the combined tectonic and loading model is summarised in Fig. 6, and the estimated absolute Euler poles for these three cases are presented in Table 4. The estimation of the absolute Euler poles and their respective rotation rates is very slightly affected (corresponding to less that ±1mm/years in computed site velocities) by the choice of a priori or null GIA model. This is predominantly due to the small magnitude of the horizontal motion in each GIA model, and the relatively small proportion of most plates that is affected. The main changes to the raw velocities will appear in the vertical direction and will not be manifested in the plate motion estimation. If the values in Table 4 are compared to values from previous studies such as Sella et al. (2002) or Altamimi et al. (2007) (Fig. 7) we see a general agreement of the location of the Euler pole, but the error ellipses of our estimates are smaller. Our error ellipses have been scaled, using Equation 32 of Bos et al. (2008) and the predicted mean power law noise of Santamaria-Gomez et al. (2011) as a guideline for calculating a confidence limit scaling factor of 20 to account for the effects of non-white noise behaviour, so they are realistic representations of the error budget. The improvement in precision compared with these earlier studies comes from the vast increase in data available and the homogeneous nature of the station time series.

A Chi-squared per degree of freedom (χ^2/DOF) test demonstrates the improvement in station velocity fit from the introduction of each GIA model. These values are summarised at the bottom of Table 4. Vertically, the introduction of either GIA model reduces the χ^2/DOF value when compared to the null GIA, which is to be expected. Horizontally, this is not the case; the χ^2/DOF value calculated after the introduction of Schotman's primary model increases in comparison to the null GIA scenario. Only Schotman's alternative model reduces the χ^2/DOF value. However, the smallest value does not necessarily correspond to the "truest" values of the Euler vectors; it is possible that the plate motion estimate in the null GIA scenario is absorbing some of the horizontal motion which is actually due to GIA. What these results highlight is that existing global GIA models, based on spherically symmetric Earth models, may poorly represent lateral velocities in individual regions. Regional GIA models with 1D Earth structure (e.g. Milne et al. 2004) may be tuned to represent both lateral and vertical velocities, but full 3D variable Earth structure is necessary for accurate modelling throughout the global domain (Latychev et al. 2005).

4.2 Periodic site displacements and solution quality

Real periodic variations to a station's position may be caused by the transportation of mass over the surface of the Earth. The exact signature of a station's time series varies on a site-

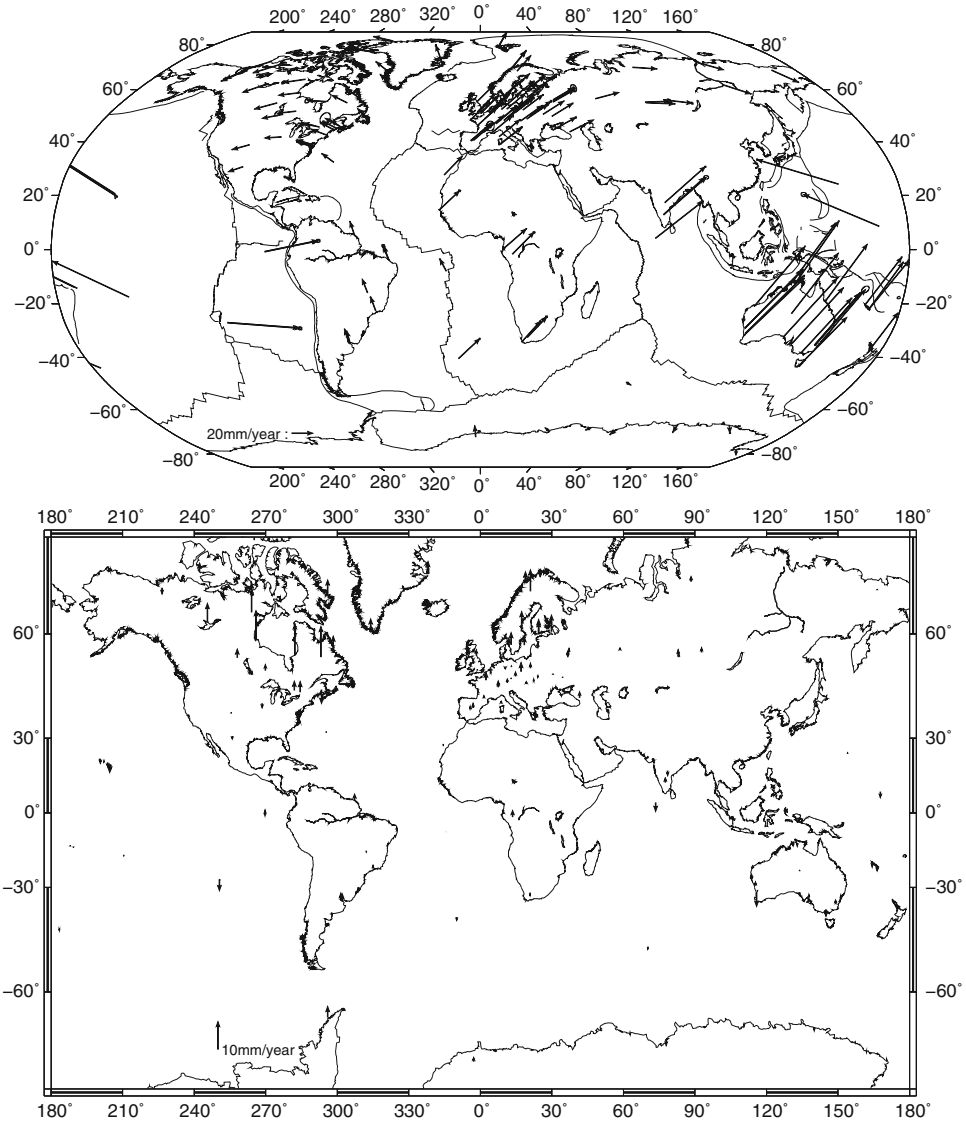

Fig. 5 Raw station velocities in the *horizontal* (*top*) and *vertical* (*bottom*) directions; *solid black lines* represent the boundaries of the tectonic plates

by-site basis, e.g. strong hydrological signals in tropical river basins (Bevis et al. 2005) or annual snowfall at high latitudes (Lidberg et al. 2007). Not all apparent signals in the GPS time series are due to geophysical causes; a non-loading signal has been identified in the GPS time series which is believed to be driven by the repetition of the satellite geometry, as it has not been found in SLR and VLBI time series (Collilieux et al. 2011; Ray et al. 2008). Periodic errors arising from model differences between analysis centres (e.g. a priori zenith hydrostatic tropospheric delay as investigated by Tregoning and Watson 2009) will be mitigated in our combined solution. Although the existence of periodic errors will have little or no effect on our velocity estimates from the long time series of the reprocessed solution, we investigate them as a demonstration of overall solution quality.

The solar year has a period of 365.25 days, but the GPS satellite geometry with respect to the Earth–Sun system repeats itself every approximately every 351.2 days, known as the GPS draconitic year. This repetition can manifest itself in the GPS time series producing a regular signal at the draconitic year (1.04 cycles per year (cpy) rather than the solar year (1 cpy), as well as its harmonics. There has been discussion about the possible origins of the draconitic periodic error (Tregoning et al. 2009): (1) local multipath due to the satellite-geometry repeating every sidereal day, for a 24 hour sampling period the alias period is the draconitic year; (2) mismodelling in the satellite orbits; or (3) errors in the a priori IERS model for the sub-daily tidal EOP variation on GPS orbits. Periods which are common to all sites, irrespective of location, may factor into the reprocessed station time series in addition to geophysical seasonal periods. The examination of individual station time series will not provide any information about systematic errors in the GPS time series as each time series will be a composition of station specific and

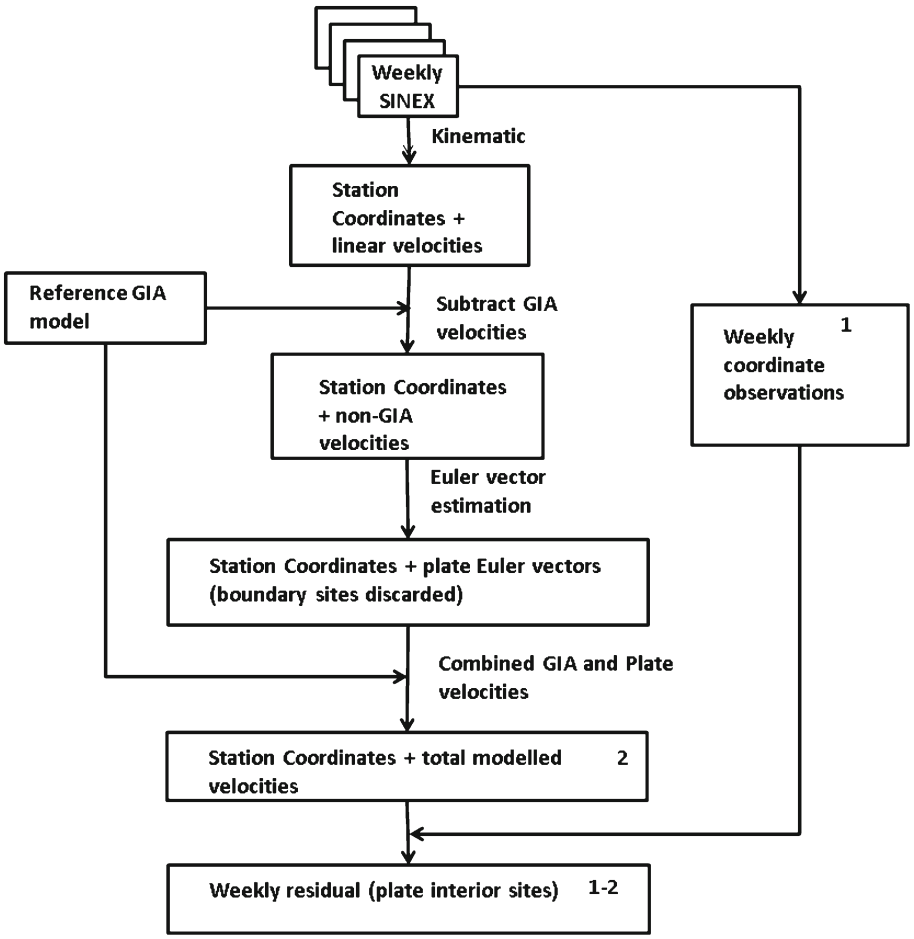

Fig. 6 Scheme of modelled velocity estimation and attribution. The weekly residual displacements with respect to the plate tectonic model (1–2) are derived from the difference between the weekly combined coordinate observations (1) and the modelled site velocities and coordinates at the reference epoch (2)

global system effects. Dong et al. (2002) estimated that less than half the power in the operational time series is driven by real seasonal signals, leaving the remaining unaccounted for. More recent analyses (e.g. Tregoning et al. 2009; Tesmer et al. 2011) show improved agreement between GPS and modelled seasonal signals, but significant discrepancies remain.

Attempts have been made by authors to identify and quantify these spurious signals in the GPS time series. Ray et al. (2008) stacked multiple global station time series power spectra using the IGS operational data, with the aim of eliminating localised geophysical signals and highlighting common (global) higher order draconitic spikes emerging above the background noise. Ray et al. (2008) found power at 1 cpy up to the 6th harmonic; however, as mentioned, these periods are not strictly harmonics of the solar period. Collilieux et al. (2011) and Ray et al. (2008) both find no evidence of similar periodic signals (3rd or higher harmonics) in results from VLBI, SLR or loading models, suggesting that they arise from a problem with the GPS data or processing as opposed to a genuine geophysical signal. Due to the sampling frequency of the reprocessed submissions (weekly) it may not be possible to distinguish between the draconitic and solar annual periods at the lower harmonics, but higher harmonics should be separable.

The spectra of station time series of the reprocessed NC1 combination were interpolated and stacked (Fig. 8). There is clear power at the annual (solar) period in all three components and at the semi-annual period in the east component; however, the semi-annual period is not so clear for the up and north components, and there is some suggestion that this peak is closer to the second draconitic harmonic. The picture becomes much clearer at the higher harmonics. The 4th and 6th harmonics clearly lie on the draconitic period harmonic with some suggestion of the 5th and 7th harmonics doing so as well. The 3rd harmonic is unclear: the up component lies on the draconitic harmonic but the horizontal values fall somewhere in between the draconitic and solar periods. What this shows is that with the reduced noise in the reprocessing solutions, the presence of spurious signals in the data set becomes more readily apparent. However, beyond demonstrating the quality of the IGS reprocessed solution, such considerations will have little effect on the secular site velocities due to the long timespan of the dataset.

Table 4 Tectonic plate absolute Euler pole estimates and χ^2/DOF of model velocities

Plate	Null	Schotman	Schotman Alt
Antarctic			
ϕ°	58.37	58.54	58.55
λ°	232.94	234.58	234.24
ω°/years	0.213	0.217	0.214
Australian	32.40	32.20	32.40
	38.03	38.12	38.01
	0.634	0.636	0.634
Eurasian	54.46	54.78	54.33
	259.44	257.90	259.30
	0.250	0.249	0.249
Indian	51.58	51.83	51.64
	1.55	0.91	1.20
	0.531	0.527	0.530
Nazca	45.95	46.42	45.94
	256.70	257.01	256.62
	0.631	0.626	0.630
North American	−4.04	−4.55	−3.55
	274.68	275.03	275.03
	0.195	0.194	0.195
Nubian	49.21	50.05	49.22
	279.19	280.42	279.68
	0.269	0.269	0.269
Pacific	−62.39	−62.62	−62.32
	111.25	111.00	111.08
	0.684	0.684	0.683
South American	−18.68	−17.84	−18.47
	229.99	228.55	229.67
	0.129	0.126	0.129
3D χ^2/DOF	3.12	1.57	2.39
Vertical χ^2/DOF	8.84	4.33	6.75
Horizontal χ^2/DOF	0.53	0.60	0.45

5 Present-day secular loading

Our final goal is the detection and quantification of present-day secular surface mass loading. This is made possible by the procedure described above in Sect. 4, which removes the identified causes of other secular deformation, i.e. GIA and plate tectonics. The residual velocities will be caused by present-day SML, assuming that there are no random model errors or velocity biases from the a priori GIA model and associated plate tectonic model, or from other causes.

5.1 Loading estimation

By fitting a set of self-gravitating, mass-conserving basis functions (Clarke et al. 2007) to the residual surface velocities (shown in the supplementary material), it is possible to estimate an equivalent column of seawater representative of SML. Our basis functions represent the coastline to spherical harmonic degree and order 45, corresponding to a spatial resolution of ∼440 km, and the surface mass load to a chosen 'level' which within the spatial domain of the land corresponds to the equivalent spherical harmonic degree and order. A vital stage of this estimation is deciding the 'level' (or number of parameters) which will be estimated. A χ^2/DOF test could be used to determine the optimum level, but a hurdle arises when calculating the effective number of degrees of freedom. As mentioned in Sect. 3.2, the distribution of tracking sites is not uniform. Some areas, such as Africa, are light in station data so there are only a few points to constrain the estimated load, leaving it free to deviate from the true value. Other areas that are well observed, such as North America or Europe, may be over-constrained, notwithstanding errors which may be regionally spatially correlated in addition to showing temporal correlation from one week to the next. The global χ^2/DOF therefore does not reflect the spatial variability of observations or the goodness of fit of a particular region, although it can still be used as a rough guideline. Generally, a χ^2/DOF value between 0.1 and 10 would heuristically be held to represent a fair model estimation with only a slight- or under-fitting, assuming correlations between observations have been correctly treated.

Table 5 shows that as the number of estimated parameters increases, with the increase of basis function level, χ^2/DOF reduces as the fit improves. Because of the large number of degrees of freedom in all cases, it is not realistic to use a standard F-test for a rigorous determination of the basis function level at which improved fit ceases to be statistically significant. As stated above, χ^2/DOF values which are within the range 0.1–10 heuristically represent a fair model fit; for most of the model/level combinations shown this is the case. However, as the network of stations is not evenly distributed over the surface of the Earth (Fig. 1), an overall reasonable χ^2/DOF can mask over-fitting in some areas or under-fitting in others. Alternatively, by examining the spatial distribution of the estimated loads it can be seen how the estimation quickly becomes unstable at higher levels (Fig. 9). Referring to the synthetic data tests of Clarke et al. (2007), we determine that a level 5 estimation should be the maximum obtainable solution for our data; despite Clarke et al. (2007) using synthetic data over a sparser network for much of their analysis, it is still comparable as there is a similar issue with the uneven distribution of the network. It is clear from Fig. 9 that as the level increases beyond 5 then the stability of the estimation soon degrades, producing estimated loads of over 3,000 mm/years for a level 8 estimation (not shown), which are clearly unrealistic. At lower levels, more plausible values are obtained. Synthetic tests demonstrate that for our site network geometry, site velocity

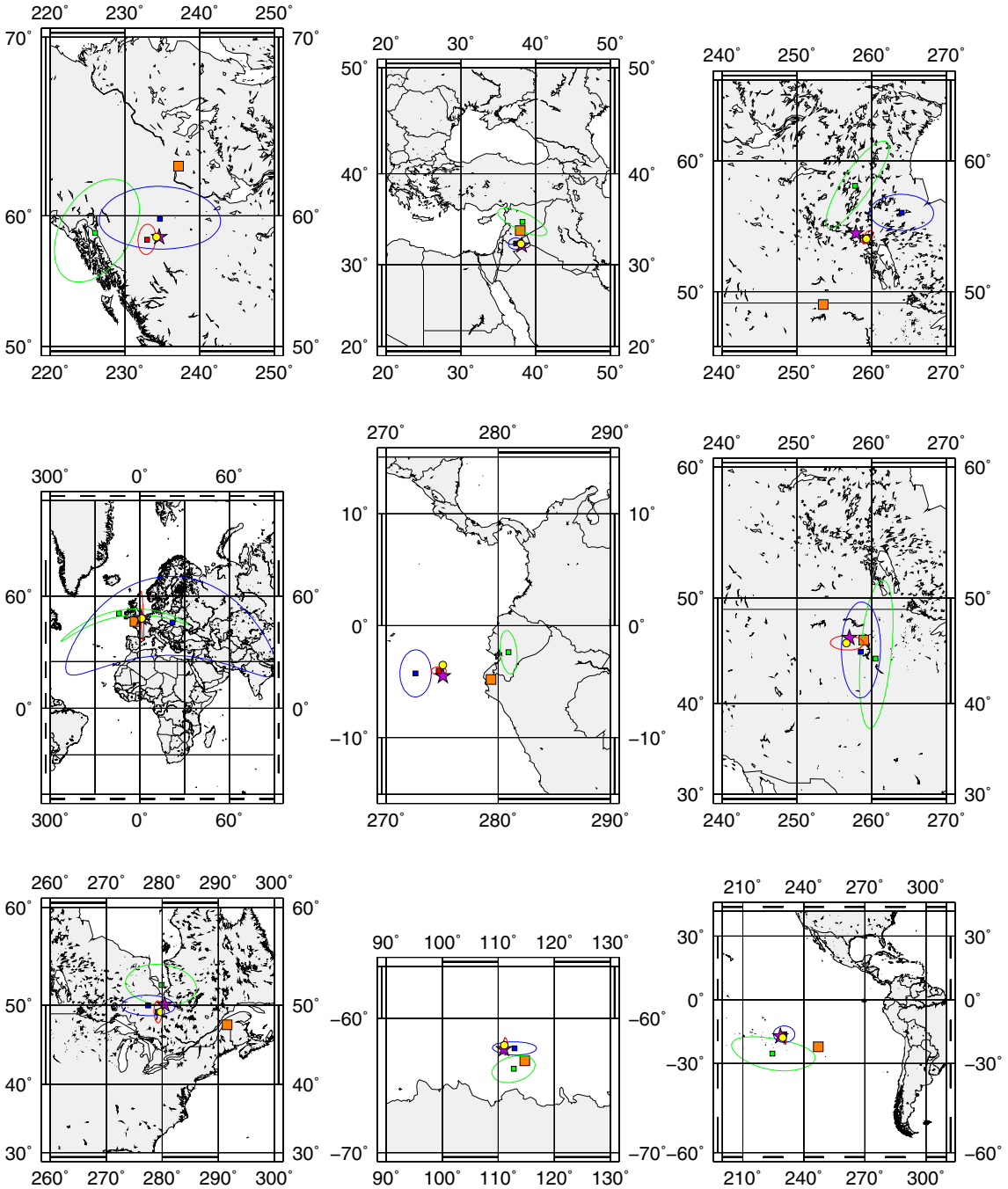

Fig. 7 Estimated plate Euler poles and 95 % confidence error ellipses. *Red square*, this solution (NC1, null GIA model); *blue square* ITRF2005; *green square* REVEL (Sella et al. 2002); *orange square* NNR-MORVEL56 (Argus et al. 2011, no error information). The *purple star* and *yellow circle* show the NC1 solution with the Schotman and Schotman Alt GIA models, respectively, (confidence limits as for NC1). *Top* row (L–R) Antarctic, Australian, Eurasian plates. *Middle row* (L–R) Indian, North American, Nazca plates. *Bottom row* (L–R) Nubian, Pacific, South American plates

biases of RMS 0.2 mm/years (horizontal) and 1 mm/years (vertical) introduce estimated load errors of <40 mm/years at basis function level 5 or below, in all areas. At higher basis function levels, estimated secular load errors exceed 100 mm/years for data-sparse areas outside of North America, Eurasia and Australia. For Africa, Arabia and southeast Asia, we are careful not to over-interpret the estimated secular SML even at basis function level 5; accordingly, we limit the discussion below to higher latitude regions. The introduction of an a priori GIA model should account for the majority of

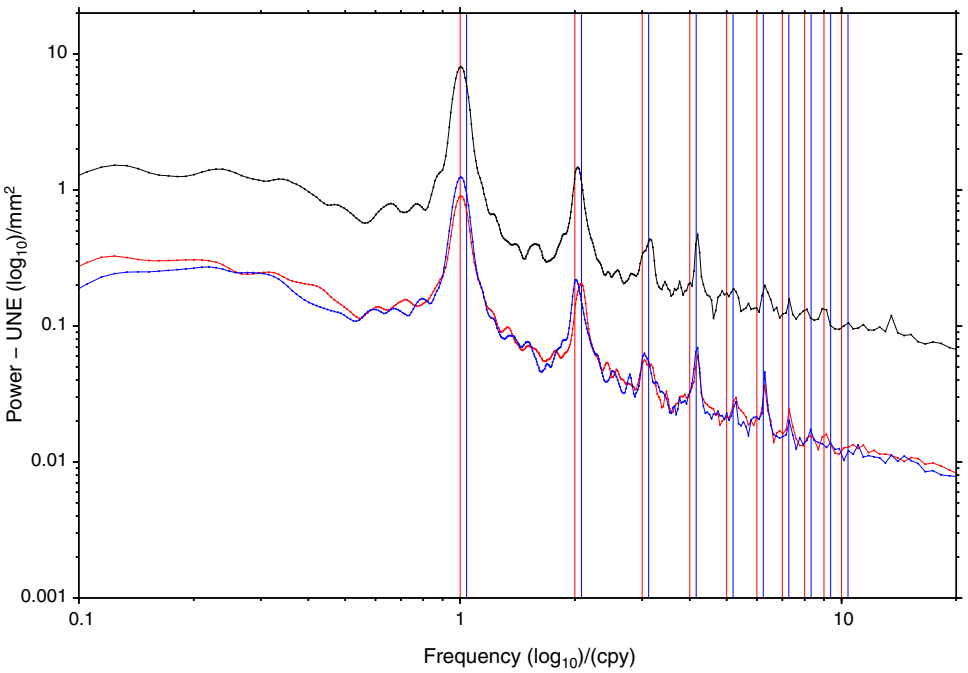

Fig. 8 Stacked periodograms of non-linear station positions (log scale): *black* (up), *red* (East) and *blue* (North). The *vertical red* and *blue lines* represent 1.0 and 1.04 cpy periods and their first 10 harmonics, respectively

Table 5 3D χ^2/DOF at an increasing basis function level

Level	1	2	3	4	5	6	7	8
3D dof	185,789	182,974	179,033	174,019	167,820	160,518	152,141	142,607
Null GIA	0.69	0.65	0.66	0.66	0.67	0.60	0.56	0.54
Schotman	1.02	0.99	0.99	0.98	0.95	0.85	0.86	0.85
Schotman Alt	0.48	0.46	0.46	0.46	0.45	0.40	0.41	0.41

All levels have 188,013 observations

true non-loading deformation observed over North America, Greenland, Europe and Antarctica. Figure 10 shows the level 5 estimation for both GIA scenarios; corresponding plots for levels 4 and 6 can be found in the supplementary material.

5.2 Mass loss estimates

We estimate secular mass change integrated over three chosen areas of topical interest: Alaska, the Antarctic Peninsula and Greenland, where comparator studies exist that have identified secular mass loss due to glacial melting. These regions have approximate surface areas of 1.48×10^6 km^2, 1.06×10^6 km^2 and 2.17×10^6 km^2, respectively (Fig. 11). For each region, we convolve a high-resolution regional mask with our estimate of the secular SML. This convolution is carried in the spatial domain, so will introduce no additional bias to the estimated load, although omission errors due to the truncation level of the original basis functions may remain. Table 6 gives the estimates of secular mass loss at different basis function levels, for the different GIA scenarios.

It is clear that our estimation is not stable for the Antarctic Peninsula due to the sparsity of GPS tracking stations in this area and the thin linear nature of the peninsula which makes it poorly represented by the basis functions. This is not the case for Alaska or Greenland as these regions are much larger and of lower aspect ratio. There is also a large variation between the different GIA models, which equals or exceeds that for the different basis function levels. Our estimates of mass loss for Greenland and Alaska have a maximum stable inversion level of 7 and 5/6, respectively; this maximum level is inferred from analysis of synthetic seasonal data which have had known site velocity biases (RMS 0.2 mm/years horizontal, 1.0 mm/years vertical) added. This same synthetic data set has been used to calculate a realistic inversion error budget.

Other authors have also attempted to use GPS, and/or GRACE, data with some form of GIA adjustment, e.g. Wu et al. (2010) estimated GIA-adjusted global mass transfer using GRACE and GPS time series and an ocean bottom pressure model. Although their results are not linked with specific GIA models as ours are, they can still be compared. For the areas considered by our study, Wu et al.

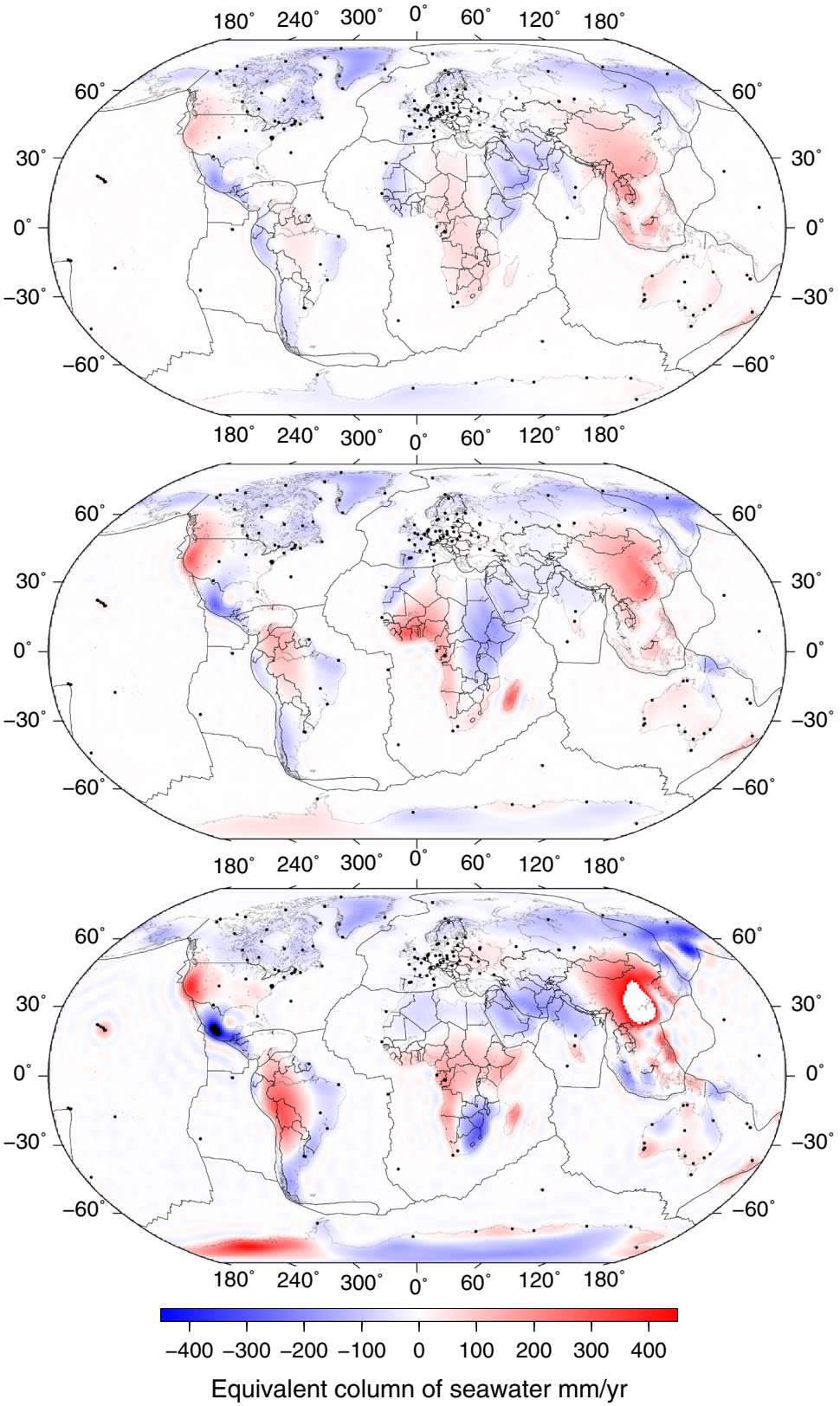

Fig. 9 Loading estimates for a null GIA model, for basis function levels 4, 5 and 6 (*top* to *bottom*), with a common *colour scale*

(2010) calculated rates of −101 ± 23 Gt/years (Alaska) and −104 ± 23 Gt/years (Greenland). This result for Alaska is about twice that of the GIA-corrected NC1 level 4–6 results (median −43 ± 30 Gt/years); however, if we consider the Wu et al. (2010) GRACE-only estimate of −68 ± 28 Gt/years this agrees broadly with the NC1 results. Over Greenland,

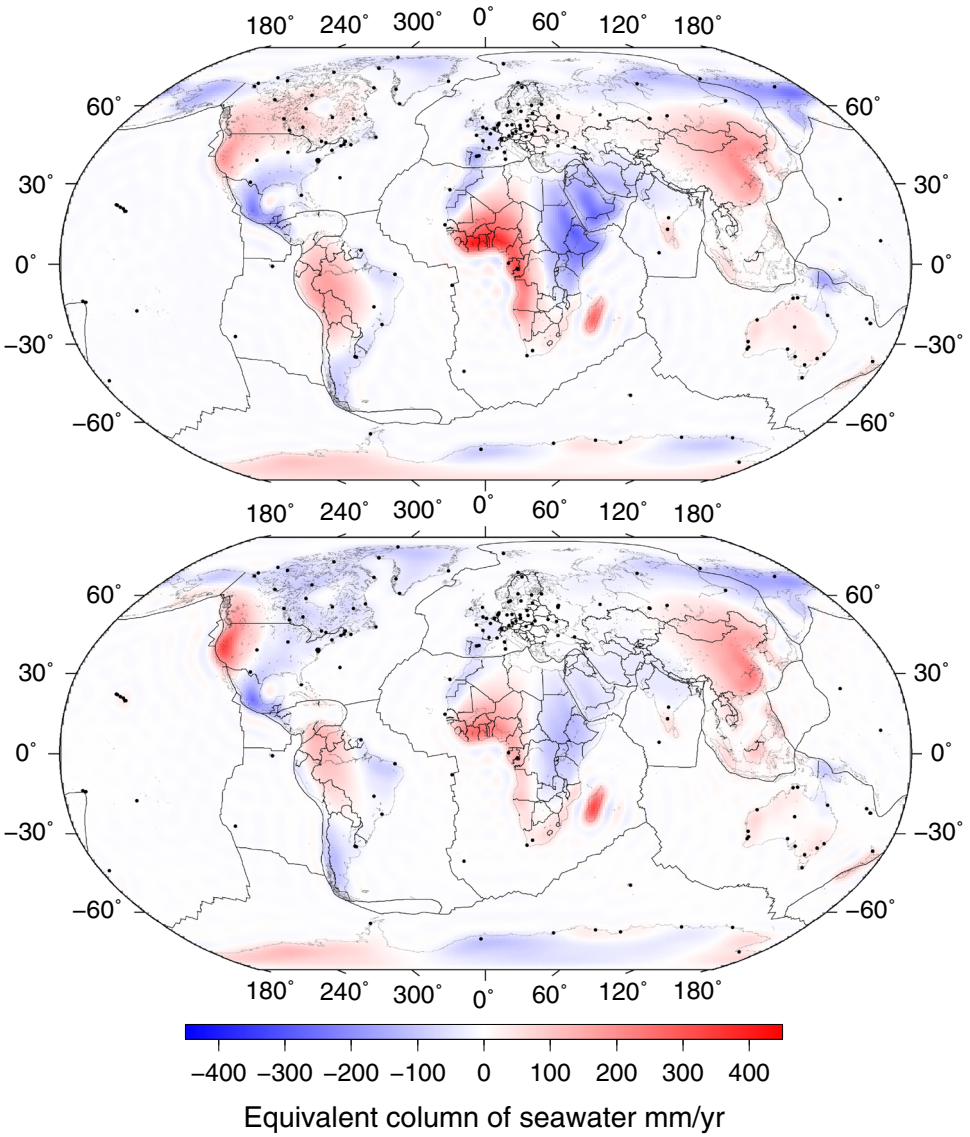

Fig. 10 Loading estimation at basis function level 5, including a GIA model: Schotman (*top*), Schotman Alternative (*bottom*)

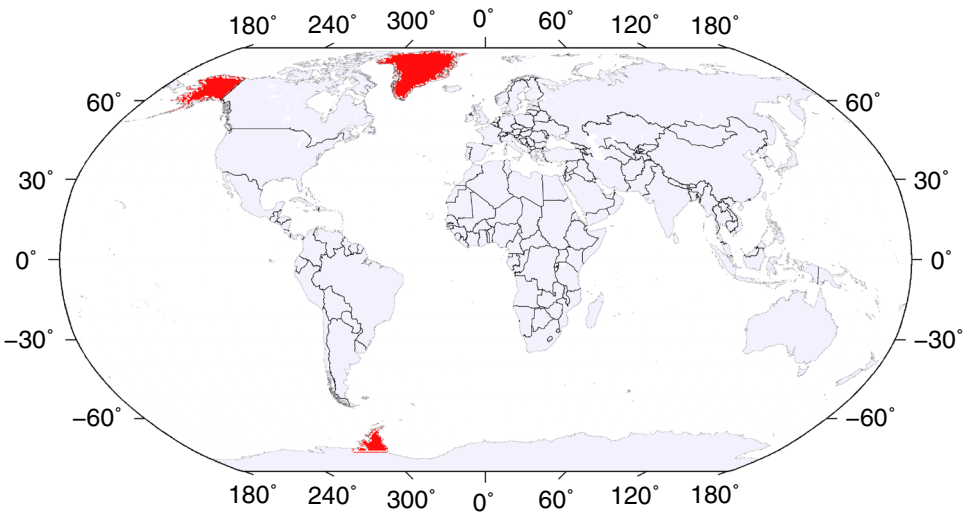

Fig. 11 Land masks used for regional mass loss estimates

Table 6 Estimated mass change in Gt/years, for basis function levels 4–7 and all GIA models, for each of the regions of interest

Alaska	4 (±18)	5 (±29)	6 (±31)	7 (±80)
Null GIA	−41	−57	−68	−123
Schotman	−49	−114	−56	−70
Schotman Alt	−37	−25	−35	−105
Greenland	4 (±12)	5 (±22)	6 (±22)	7 (±35)
Null GIA	−245	−194	−226	−195
Schotman	−90	−79	−140	−135
Schotman Alt	−188	−113	−148	−135
Antarctic Peninsula	4 (±6)	5 (±7)	6 (±25)	7 (±45)
Null	−12	15	−11	48
Schotman	−12	12	53	90
Schotman Alt	−10	7	18	64

The 1σ error budget derived from the synthetic data tests described in the text is shown in brackets for each level

Wu et al. (2010) infer a slightly larger mass loss than the median GIA-corrected level 4–6 NC1 result of -127 ± 22 Gt/years, but insignificantly so at 1σ confidence. Newer GPS-GRACE estimates using a higher truncation level (X. Wu, pers. comm., 2014) of -144 ± 28 Gt/years for Greenland and -123 ± 28 Gt/years for Alaska are in closer and worse agreement, respectively. Luthcke et al. (2013) used a GRACE mascon approach to infer total mass loss of -71 ± 11 Gt/years in Alaska and -226 ± 12 Gt/years for Greenland. Shepherd et al. (2012) also inspected the Greenland ice sheet and estimated a mass loss of -142 ± 49 Gt/years which broadly matches our result. Comparing our results to recent work by King et al. (2012) who, using GRACE data and updated GIA models, present new evidence for a significantly reduced estimate of mass loss from Antarctica may suggest that our dismissal of the Peninsula results is overly cautious. Work presented by Shepherd et al. (2012) also suggests a reduced value for the Antarctic Peninsula.

If our median results (excluding basis function level 7) are compared with those for Greenland purely from GRACE mission data (Table 7) then we see that our estimates (median -127 ± 22 Gt/years after correction for GIA) fall within the range of the latter. On its own GRACE is also unable to distinguish between present-day surface mass loss and GIA, therefore any studies of present-day secular mass loss must be adjusted by introducing a GIA model. The values from our study are consistent with the middle of the range of these published results, but the dependence of both GRACE and GPS results on GIA models further highlights the need for robust GIA modelling.

6 Conclusions

The precision of station coordinates from GPS measurements is continually improving. This is predominantly due to ongoing efforts to improve processing strategies, and the ever-increasing network of high-quality tracking stations. The first IGS reprocessing campaign has resulted in an improved kinematic solution with the inclusion of additional stations over the 11-year period studied here. This improvement is highlighted in the reduction of the weekly combined network WRMS, the reductions in noise in the Helmert transformation parameters of the combined solution, and the reduced error bounds of the absolute Euler pole estimation.

Careful steps have been taken to integrate a fully consistent GIA and tectonic plate model to obtain a single 3D secular loading deformation model. The estimate of plate tectonic Euler poles has been shown to be insensitive to the removal of the a priori GIA model, but the loading model is improved when compared to the null GIA scenario. Significant differences exist between the secular loading mod-

Table 7 GIA-adjusted mass loss estimated from GRACE over Greenland (Gt/years)

Study	GIA model	Data span	Mass loss
Velicogna and Wahr (2005)	ICE5G-VM2	April 2002–July 2004	-82 ± 28
Velicogna and Wahr (2006)	ICE5G-VM2	April 2002–April 2006	-248 ± 36
Chen et al. (2006)	ICE5G-VM2	April 2002–November 2005	-234 ± 24
Luthcke et al. (2006)	ICE5G-VM2	July 2003–July 2005	-113 ± 17
Luthcke et al. (2013)	ICE5G-VM2	December 2003–November 2010	-226 ± 12
Ramillien et al. (2008)	ICE4G-VM2	July 2002–March 2005	-141 ± 16
Wouters et al. (2008)	Paulson et al. (2005)	February 2003–January 2008	-179 ± 25
Velicogna (2009)	ICE5G-VM2	April 2002–February 2009	-230 ± 33
Pritchard et al. (2011)	ICE5G-VM2	2004–2009	-66 ± 49
Wu et al. (2010) updated (pers. comm.)	Estimated	2002–2008	-144 ± 28
NC1 (this paper)	Schotman/Alt	1999–2010	-127 ± 22

els inferred using different GIA models. We have shown that using land-masked, mass-conserving basis functions it is possible to estimate present-day secular surface mass loading at global and regional scales, using GPS coordinate data only. These results are comparable to independent estimates from the GRACE mission. Further improvements in spatial resolution and accuracy will require densification of the GPS tracking network and improvements in GIA modelling.

Acknowledgments This work was funded by NERC grant NE/E017495/1 to PJC and DAL, and by a NERC PhD studentship (associated with grant NE/E007023/1) to DB. It would not have been possible without the continued effort of all the IGS contributors producing freely accessible and high quality GPS data and analysis. We thank X. Wu, P. Tregoning and an anonymous reviewer for their constructive criticism.

References

Altamimi Z, Collilieux X, Legrand J, Garayt B, Boucher C (2007) ITRF2005: a new release of the International Terrestrial Reference Frame based on time series of station positions and earth orientation parameters. J Geophys Res Solid Earth 112(B9). doi:10.1029/2007JB004949

Altamimi Z, Collilieux X, Metivier L (2011) ITRF2008: an improved solution of the international terrestrial reference frame. J Geod 85(8):457–473

Argus DF, Gordon RG, DeMets C (2011) Geologically current motion of 56 plates relative to the no-net-rotation reference frame. Geochem Geophys Geosyst 12(11). doi:10.1029/2011GC003751

Arriagada C, Arancibia G, Cembrano J, Martinez F, Carrizo D (2011) Nature and tectonic significance of co-seismic structures associated with the mw 8.8 Maule earthquake, central-southern Chile forearc. J Struct Geol 33(5):891–897

Bennett RA (2008) Instantaneous deformation from continuous GPS: contributions from quasi-periodic loads. Geophys J Int 174(3):1052–1064

Bevis M, Alsdorf D, Kendrick E, Fortes LP, Forsberg B, Smalley R, Becker J (2005) Seasonal fluctuations in the mass of the Amazon River system and Earth's elastic response. Geophys Res Lett 32:L16308

Blewitt G, Clarke P (2003) Inversion of Earth's changing shape to weigh sea level in static equilibrium with surface mass redistribution. J Geophys Res Solid Earth 108(B6). doi:10.1029/2002JB002290

Blewitt G, Heflin MB, Webb FH, Lindqwister UJ, Malla RP (1992) Global coordinates with centimeter accuracy in the international terrestrial reference frame using GPS. Geophys Res Lett 19(9):853–856

Blewitt G, Lavallee D (2002) Effect of annual signals on geodetic velocity. J Geophys Res Solid Earth 107(B7). doi:10.1029/2001JB000570

Blewitt G, Lavallee D, Clarke P, Nurutdinov K (2001) A new global mode of Earth deformation: seasonal cycle detected. Science 294(5550):2342–2345

Boehm J, Werl B, Schuh H (2006) Troposphere mapping functions for GPS and very long baseline interferometry from European Centre for Medium-range weather forecasts operational analysis data. J Geophys Res Solid Earth 111(B2). doi:10.1029/2005JB003629

Bos MS, Fernandes RMS, Williams SDP, Bastos L (2008) Fast error analysis of continuous GPS observations. J Geod 82(3):157–166

Chen C-H, Yeh T-K, Liu J-Y, Wang C-H, Wen S, Yen H-Y, Chang S-H (2011) Surface deformation and seismic rebound: implications and applications. Surv Geophys 32(3):291–313

Chen JL, Wilson CR, Tapley BD (2006) Satellite gravity measurements confirm accelerated melting of Greenland ice sheet. Science 313(5795):1958–1960

Clarke PJ, Lavallee DA, Blewitt G, van Dam T (2007) Basis functions for the consistent and accurate representation of surface mass loading. Geophys J Int 171(1):1–10

Collilieux X, Metivier L, Altamimi Z, van Dam T, Ray J (2011) Quality assessment of GPS reprocessed terrestrial reference frame. GPS Solut 15(3):219–231

Cretaux JF, Soudarin L, Davidson FJM, Gennero MC, Berge-Nguyen M, Cazenave A (2002) Seasonal and interannual geocenter motion from SLR and DORIS measurements: comparison with surface loading data. J Geophys Res Solid Earth 107(B12). doi:10.1029/2002JB001820

Davies P, Blewitt G (2000) Methodology for global geodetic time series estimation: a new tool for geodynamics. J Geophys Res Solid Earth 105(B5):11083–11100

Davis JE, Latychev K, Mitrovica JX, Kendall R, Tamisiea ME (2008) Glacial isostatic adjustment in 3-D Earth models: implications for the analysis of tide gauge records along the US east coast. J Geodyn 46(3):90–94

Dong D, Fang P, Bock Y, Cheng MK, Miyazaki S (2002) Anatomy of apparent seasonal variations from GPS-derived site position time series. J Geophys Res Solid Earth 107(B4). doi:10.1029/2001JB000573

Dow J, Neilan R, Rizos C (2009) The international GNSS service in a changing landscape of global navigation satellite systems. J Geod 83:191–198

Farrell WE, Clark JA (1976) Postglacial sea-level. Geophys J Royal Astron Soc 46(3):647–667

Ferland R, Piraszewski M (2009) The IGS-combined station coordinates, Earth rotation parameters and apparent geocenter. J Geod 83(3–4):385–392

Kendall RA, Latychev K, Mitrovica JX, Davis JE, Tamisiea ME (2006) Decontaminating tide gauge records for the influence of glacial isostatic adjustment: the potential impact of 3-D Earth structure. Geophys Res Lett 33(24). doi:10.1029/2006GL028448

Khan SA, Wahr J, Leuliette E, van Dam T, Larson KM, Francis O (2008) Geodetic measurements of postglacial adjustments in Greenland. J Geophys Res Solid Earth 113(B2). doi:10.1029/2007JB004956

King MA, Altamimi Z, Boehm J, Bos M, Dach R, Elosegui P, Fund F,Hernandez-Pajares M, Lavallee D, Cerveira PJM, Penna N, Riva REM,Steigenberger P, van Dam T, Vittuari L, Williams S, Willis P (2010) Improved constraints on models of glacial isostatic adjustment: a review of the contribution of ground-based geodetic observations. Surv Geophys 31:465–507

King MA, Bingham RJ, Moore P, Whitehouse PL, Bentley MJ, Milne GA (2012) Lower satellite-gravimetry estimates of Antarctic sea-level contribution. Nature 491(7425):586–589

Kogan MG, Steblov GM (2008) Current global plate kinematics from GPS (1995–2007) with the plate-consistent reference frame. J Geophys Res Solid Earth 113(B4). doi:10.1029/2007JB005353

Kreemer C, Haines J, Holt WE, Blewitt G, Lavallee D (2000) On the determination of a global strain rate model. Earth Planets Space 52(10):765–770

Larson KM, Freymueller JT, Philipsen S (1997) Global plate velocities from the global positioning system. J Geophys Res Solid Earth 102(B5):9961–9981

Latychev K, Mitrovica JX, Tamisiea ME, Tromp J, Christara CC, Moucha R (2005) GIA-induced secular variations in the Earth's long wavelength gravity field: influence of 3-D viscosity variations. Earth Planet Sci Lett 240:322–327

Lidberg M, Johansson JM, Scherneck H-G, Davis JL (2007) An improved and extended GPS-derived 3D velocity field of the glacial isostatic adjustment (GIA) in Fennoscandia. J Geod 81(3):213–230
Love A (1909) The yielding of the Earth to disturbing forces. Proc Royal Soc Ser A 82:73–88
Luthcke SB, Sabaka TJ, Loomis BD, Arendt AA, McCarthy JJ, Camp J (2013) Antarctica, Greenland and Gulf of Alaska land-ice evolution from an iterated GRACE global mascon solution. J Glaciol 59(216). doi:10.3189/2013JoG12J147
Luthcke SB, Zwally HJ, Abdalati W, Rowlands DD, Ray RD, Nerem RS, Lemoine FG, McCarthy JJ, Chinn DS (2006) Recent Greenland ice mass loss by drainage system from satellite gravity observations. Science 314(5803):1286–1289
McCarthy D, Petit G (2004) IERS conventions 2003. IERS Technical Note 32
Milne GA, Mitrovica JX, Scherneck H-G, Davis JL, Johansson JM, Koivula H, Vermeer M (2004) Continuous GPS measurements of postglacial adjustment in Fennoscandia: 2. Modelling results. J Geophys Res 109:B02412
Mitrovica JX, Davis JL, Shapiro II (1994) A spectral formalism for computing three-dimensional deformations due to surface loads: 2. Present-day glacial isostatic adjustment. J Geophys Res 99(B4):7075–7101
Paulson A, Zhong SJ, Wahr J (2005) Modelling post-glacial rebound with lateral viscosity variations. Geophys J Int 163(1):357–371
Pritchard HD, Luthcke SB, Fleming AH (2011) Understanding ice-sheet mass balance: progress in satellite altimetry and gravimetry. J Glaciol 56(200):1151–1161
Ramillien G, Famiglietti JS, Wahr J (2008) Detection of continental hydrology and glaciology signals from GRACE: a review. Surv Geophys 29(4–5):361–374
Ray J, Altamimi Z, Collilieux X, van Dam T (2008) Anomalous harmonics in the spectra of GPS position estimates. GPS Solut 12(1):55–64
Ray J, Dong D, Altamimi Z (2004) IGS reference frames: status and future improvements. GPS Solut 8:251–266
Reddy CD, Arora SK, Sunil PS, Prajapati SK (2011) Earthquake related deformation cycle: perspectives from 2004 Sumatra and 2010 Chile mega-earthquakes. Disaster Adv 4(2):13–21
Santamaria-Gomez A, Bouin M-N, Collilieux X, Woeppelmann G (2011) Correlated errors in GPS position time series: Implications for velocity estimates. J Geophys Res Solid Earth 116. doi:10.1029/2010JB007701
Schaer S (2006) Determination and use of GPS differential code bias values. IGS Technical Workshop, Darmstadt
Schmid R, Mader G, Herring T (2005) From relative to absolute antenna phase centre corrections. IGS Technical Workshop, Berne
Schotman HHA, Wu P, Vermeersen LLA (2008) Regional perturbations in a global background model of glacial isostasy. Phys Earth Planet Interiors 171(1–4):323–335
Sella GF, Dixon TH, Mao AL (2002) REVEL: a model for recent plate velocities from space geodesy. J Geophys Res Solid Earth 107(B4). doi:10.1029/2000JB000033
Shepherd A, Ivins ER, Geruo A, Barletta VR, Bentley MJ, Bettadpur S, Briggs KH, Bromwich DH, Forsberg R, Galin N et al (2012) A reconciled estimate of ice-sheet mass balance. Science 338(6111):1183–1189
Tesmer V, Steigenberger P, van Dam T, Mayer-Gurr T (2011) Vertical deformations from homogeneously processed GRACE and global GPS long-term series. J Geod 85:291–310
Tregoning P, Watson C (2009) Atmospheric effects and spurious signals in GPS analyses. J Geophys Res 114:B09403
Tregoning P, Watson C, Ramillien G, McQueen H, Zhang J (2009) Detecting hydrologic deformation using GRACE and GPS. Geophys Res Lett 36. doi:10.1029/2009GL038718
Tushingham AM, Peltier WR (1991) ICE-3G: a new global model of late Pleistocene deglaciation based upon geophysical predications of postglacial relative sea level change. J Geophys Res 96:4497–4523
van Dam T, Wahr J, Lavallee D (2007) A comparison of annual vertical crustal displacements from GPS and gravity recovery and climate experiment (GRACE) over Europe. J Geophys Res Solid Earth 112(B3). doi:10.1029/2006JB004335
van Dam T, Wahr J, Milly PCD, Shmakin AB, Blewitt G, Lavallee D, Larson KM (2001) Crustal displacements due to continental water loading. Geophys Res Lett 28(4):651–654
van Dam TM, Francis O (1998) Two years of continuous measurements of tidal and nontidal variations of gravity in Boulder, Colorado. Geophys Res Lett 25(3):393–396
Velicogna I (2009) Increasing rates of ice mass loss from the Greenland and Antarctic ice sheets revealed by GRACE. Geophys Res Lett 36. doi:10.1029/2009GL040222
Velicogna I, Wahr J (2005) Greenland mass balance from GRACE. Geophys Res Lett 32(18). doi:10.1029/2005GL023955
Velicogna I, Wahr J (2006) Measurements of time-variable gravity show mass loss in Antarctica. Science 311(5768):1754–1756
Wahr J, van Dam T, Larson K, Francis O (2001) GPS measurements of vertical crustal motion in Greenland. J Geophys Res Atmos 106(D24):33755–33759
Wouters B, Chambers D, Schrama EJO (2008) GRACE observes small-scale mass loss in Greenland. Geophys Res Lett 35(20). doi:10.1029/2008GL034816
Wu X, Heflin MB, Schotman H, Vermeersen BLA, Dong D, Gross RS, Ivins ER, Moore A, Owen SE (2010) Simultaneous estimation of global present-day water transport and glacial isostatic adjustment. Nat Geosci 3(9):642–646
Wu XP, Argus DF, Heflin MB, Ivins ER, Webb FH (2002) Site distribution and aliasing effects in the inversion for load coefficients and geocenter motion from GPS data. Geophys Res Lett 29(24). doi:10.1029/2002GL016324
Wu XP, Heflin MB, Ivins ER, Argus DF, Webb FH (2003) Large-scale global surface mass variations inferred from GPS measurements of load-induced deformation. Geophys Res Lett 30(14). doi:10.1029/2003GL017546